Supplementary Information for

Sustained wood burial in the Bengal Fan over the last 19 million years

Hyejung Lee, Valier Galy, Xiaojuan Feng, Camilo Ponton, Albert Galy, Christian France-Lanord,

Sarah J. Feakins

Sarah J. Feakins
Email: feakins@usc.edu

This PDF file includes:

Supplementary text
Figs. S1 to S7
References for SI reference citations

Other supplementary materials for this manuscript include the following:

Datasets S1 to S6

www.pnas.org/cgi/doi/10.1073/pnas.1913714116

SI Extended methods

Following the discovery of visible wood on split core surfaces, we collected 95 wood samples in total from six sediment cores. We sampled 58 horizons where wood pieces were directly sampled from split core surfaces. In addition, we targeted 73 similar coarse grained sediment samples (collecting sample sizes ranging from 11 to 77 g) and sieved those samples (>1 mm) to pick wood fragments not visible at the core surface. Sections of turbidites (sub-unit Ta through Td of the Bouma sequence) with coarse grains and other beds with black-colored particles were selected for sampling. Sample spacing is therefore not uniform. instead we targeted our sampling to inventory horizons that are likely wood-bearing. We endeavored to sample for buried wood across the 19 Myr sedimentary record. However, there may be additional wood in the cores not recovered by our approach. This wood inventory is likely also an underestimate of buried wood horizons as coarse, sandy sediments typically have lower drill-core recovery than fine grained sediments (core recovery is illustrated on Fig. S2). Chemical analyses were performed on aliquots from each wood horizon where sufficient wood was recovered. Measurements were performed on a variable number of fragments (1 to >100 pieces of wood), in order to obtain sufficient mass for each analysis and this necessarily depended on the size of fragments in the horizon. In some cases, a measurement derives from a single fragment and therefore a single plant, in other cases an analysis represents an average of many small fragments, i.e. likely many plants.

Bulk wood elemental and isotopic analyses

For bulk wood C and $\delta^{13}C$ analyses, 50 to 100 µg of ground wood was treated with 4% hydrochloric acid (HCl) at 85ºC for 1 h to remove carbonate, before measurement on a modified EuroEA3028-HT elemental analyzer coupled to a GV Instruments IsoPrime continuous-flow isotope mass spectrometer. OC was corrected for loss during acidification. Although samples were freeze-dried before picking and grinding wood samples, water absorption from a humid atmosphere may be an additional explanation for lower than expected C%, in addition to matrix dilution and degradation during burial. Calibration to the LVSEC/VPDB isotopic scale was achieved with two internal standards in mineral matrix and a third standard run unknown to assess accuracy. The $\delta^{13}C$ results were accurate and precise to better than 0.3‰.

Lignin methoxy hydrogen isotopic analyses

For lignin methoxy isotopic analyses, 20 to 80 mg of powdered wood was reacted with 0.1 – 0.15 mL of hydroiodic acid (HI, 55%) in the 2 mL GC vials with Al crimp caps with PTFE/rubber TF2 septum gas tight septa. Samples were heated at 120ºC for 30 min and shielded from light. Vials were cooled and held at ambient conditions ~22ºC for at least 30 min to allow the iodomethane product to equilibrate into headspace. Samples were neutralized via the

injection of 0.15 mL 5 M potassium hydroxide (KOH) through the septum with additional 0.05 – 0.1 mL until neutralized (as detected by color change). Liquid – liquid extraction was performed to partition the iodomethane into isooctane, the organic phase. 250 μL of isooctane was injected into the vial through the septum after neutralization. The mixture was vigorously shaken for 30 sec, centrifuged to facilitate separation into organic and aqueous layers. The organic phase containing iodomethane was extracted by syringe (1 – 3 times) and the fractional volume recovery was recorded, following the methods of (1).

The $\delta D_{methoxy}$ was determined at USC using a Trace gas chromatograph (GC) connected via a GC–Isolink pyrolysis furnace (at 1400°C), passing through a cold trap, and a Conflo IV interface to Delta VPlus IRMS. The GC was fitted with a ZB-5 ms column (30 m × 0.25 mm × 1 μm) and for the liquid method, 1-2 mL of isooctane containing iodomethane was injected using a gas tight syringe into a split/splitless (SSL) inlet operated at constant temperature (200°C) in splitless mode. The flow rate was at 3 mL min^{-1} with the oven temperature starting at 33°C, held for 2.5 min, followed by a 20°C min^{-1} ramp up to 130°C which was held for 0.6 min to elute the isooctane. The GC Isolink backflush multi-functional valve controller (MFVC) was heated to 65ºC, necessary to aid expulsion of isooctane.

Four peaks of hydrogen reference gas bracket the iodomethane analyte peak during the GC-isotope ratio mass spectrometer (IRMS) run. One of the initial peaks was used for standardization of the isotopic analyses, while the other three bracketing peaks were treated as unknowns (precision averaged 0.4‰, 1σ, n = 208). The known reference peak was set by comparing with an external standard (A6mix) obtained from A. Schimmelmann, Indiana University, Bloomington, containing 15 *n*-alkane compounds (C_{16} to C_{30}), with δD values spanning –9 to –254‰. The RMS error determined by replicate measurements of the standard across the course of analyses was 4.2‰. Data were then normalized to the Vienna Standard Mean Ocean Water / Standard Light Antarctic Precipitation (VSMOW/SLAP) isotopic scale by comparison with both the A6mix and an external standard of 99.7% purity CH_3I analyzed by offline combustion and analysis by dual inlet IRMS with δD values –95.6‰, 1σ 1.6‰, n = 6 (the δD value was analyzed and supplied by A. Schimmelmann, Indiana University, Bloomington). Three additional in-house reference materials (USC Lignin, Bamboo, Poplar (-254‰, -187‰, and -330‰, respectively; available from S. Feakins upon request) were run to monitor for consistency, following the principle of like substrate to sample.

Lignin phenol characterization

Lignin derived phenols were released using copper (II) oxide (CuO) oxidation method (2, 3). Briefly, wood samples (20-100 mg) were mixed with 0.5-1 g CuO, 200 mg ammonium iron (II) sulfate hexahydrate [$Fe(NH_4)_2(SO_4)_2 \cdot 6H_2O$] and 20 mL of nitrogen-purged sodium hydroxide (NaOH) solution (2 M) in teflon-lined bombs. All bombs were flushed with nitrogen in the

headsapce for 10 min and heated at 150°C for 2.5 h. The lignin oxidation products (LOPs) were spiked with a surrogate standard (ethyl vanillin), acidified to pH 1 with 6 M HCl, and kept in the dark for 1 h. After centrifugation (2500 rpm, 30 min), LOPs were liquid-liquid extracted from the clear supernatant with ethyl acetate, and concentrated under nitrogen. LOPs were derivatized with N,O-bis-(trimethylsilyl) trifluoroacetamide (BSTFA) and pyridine (70°C, 1 h) to yield trimethylsilyl (TMS) derivatives before quantification. Lignin phenols were identified and quantified on a Trace 1310 gas chromatograph coupled to an ISQ mass spectrometer (Thermo Fisher Scientific, USA) using a DB-5MS column (30 m × 0.25 mm i.d., film thickness, 0.25 μm). The oven temperature was held at 65°C for 2 min, increased from 65 to 300°C at a rate of 6°C min^{-1} with final isothermal hold at 300°C for 20 min. Helium was used as carrier gas (0.8 mL min^{-1}). The mass spectrometer was operated in the electron impact mode (EI) at 70 eV and scanned from 50 to 650 daltons. Quantification was achieved by comparing with surrogate standards to account for compound loss during extraction procedures. External quantification standards were used to normalize the response factor for different lignin phenols separately. Vanillyl (vanillin, acetovanillone, vanillic acid), syringyl (syringaldehyde, acetosyringone, syringic acid), and cinnamyl (*p*-coumaric acid, ferulic acid) phenols were summarized to represent lignin phenols.

SI Extended supplementary data discussion

Organic carbon content in wood

Wood fragments yielded C% from 3.9 to 81.4% (mean 33.5%, 1σ = 14.0, n = 257) and C/N from 18 – 189 (mean 57, 1σ = 24, n = 146, Dataset S3). We found a correlation between C% and C/N (r^2 = 0.56, p<0.05), but no correlation between C% and $\delta^{13}C_{wood}$ nor N% with $\delta^{13}C_{wood}$ (Fig. S5). Measurements with CO_2 pulses <10x blank were excluded (n = 13), N_2 peaks were low for most samples (<10x blank) which may bias C/N results to high values but we did not find a strong dependence of N% and C/N to the N peak area. Measurements with N_2 pulses <2x blank were excluded (n=23).

In tropical and temperate living trees, wood C% is typically within the range of 40 – 55% (4) and C/N is typically > 20 (5). Low C (<40%, n=161) together with low C/N (<20, n=1) was observed in a few buried wood fragments. Contamination by marine OC (low C/N) is assumed to be negligible within coarse grain turbiditic layers that contain minimal non-wood OC. Low C in fossil wood could be due to dilution by mineral matrix embedded within fragments. Minerals such as biotite can be relatively enriched in N compared to C, lowering C% and C/N without affecting $\delta^{13}C_{wood}$ values. Alternatively, water adsorption in lab processing prior to analysis may be a driver of low C without lowering of the C/N ratio from that expected from living plants or without altering $\delta^{13}C$ values. High C (~80%) was found in a 3 fragments picked from the core face across 16-97cm from U1455C 43R 2W, dated to 9.7 Ma, indicative of charred wood.

Mid-Miocene Climatic Optimum

Strong monsoonal precipitation is a seasonal driver of physical erosion in South and East Asia. High sedimentation rates in the South China Sea (6) and the incision of the Mekong River (7) have been interpreted as a strengthening of the monsoon during the Mid Miocene Climatic Optimum (MMCO), between 17 – 14 Ma. Our sampling does not reveal evidence for increased wood export at the MMCO, nor a change in the characteristics of wood exported, however we find coarse woody material has been mobilized in frequent woody layers within the 18 – 17 and 12 – 11 Ma bins.

During the MMCO, atmospheric composition experienced a rise in pCO_2 and $\delta^{13}C_{atm}$, with several carbon maxima, including four ~1‰ carbon isotope excursions between 16 and 13 Ma detected by benthic foraminifera (8). No anomaly is observed in the $\delta^{13}C_{wood}$ record (Fig. 2), suggesting that the magnitude of the atmospheric variability was small compared to other sources of variability in wood composition exported in this system, or that those carbon maxima were not captured in our record. Indeed, we did not recover much wood during the MMCO – a couple of visible horizons were picked and a couple of sieved horizons yielded wood but another set of sieved horizons were barren. We may simply have not captured wood exports of this age

as there was low sediment recovery in coring during this time. Or there may be changes in the locus of deposition within the fan, mechanism for sediment delivery (e.g. retention on the shelf during the sea level highstand), or enhanced degradation may have attenuated wood export. But, river transport velocities and discharge should have been high as the MMCO was likely warm and wet and the nearby Mekong River incision increased during the MMCO (7), thus the lack of clear response in the buried wood record is perhaps surprising. We hypothesize that during the MMCO wood export by the G-B would have continued or perhaps increased, and yet there may have been more shelf retention. But, as we do not clearly detect any wood abundance or compositional changes associated with the MMCO, we do not highlight this possibility further, as it is inferred from low wood amounts which are always ephemeral, and the observed low could readily be stochastic.

Pleistocene regime of climate variability and enhanced physical erosion

Pleistocene (last 2.6 Ma) glacial cycles witnessed global variations in temperatures, ice volume, sea level, and atmospheric composition. We do not recover much wood between 4 and 1 Ma, but we recover many wood horizons from the multiple cores collected by Exp 354 spanning the last 1 Ma during intensified glacial cycles. We observe a 19‰ range in the $\delta^{13}C$ values of wood sampled from the Bengal Fan across the last 1 Ma. Atmospheric changes included up to 100 ppm pCO_2 variations (9) and up to 1‰ variations in $\delta^{13}C_{atm}$ recorded in ancient atmospheres trapped in ice core bubbles spanning the complete last glacial cycle (10). Although there is some variability in $\delta^{13}C_{atm}$ (~1‰), this is unlikely to be a significant driver of the observed patterns in $\delta^{13}C_{wood}$, as we observe much larger swings associated with C_3 and C_4 plant types.
The direct effects of $\delta^{13}C_{atm}$ variations (the substrate for photosynthesis) are a minor contributor (1‰) to that 19‰ $\delta^{13}C_{wood}$ signal. Wood carbon isotopic values indicate a bimodal composition including C_3 and C_4 plants. This variability likely reflects changing plant communities with varying proportions of C_4 plant responding to glacial-interglacial pCO_2 and climate variability, similar to the signal of C_4 expansion captured by plant wax carbon isotopic compositions in the proximal fan during the last glacial cycle (11).

In addition, we expect there to be shifting mechanisms and loci of erosion that moves wood out of the catchment associated with Pleistocene climatic change. Although monsoonal flooding, cyclones and landslides would be ever-present mechanisms of erosion, the Pleistocene saw glacier advance and retreat (12) presumably with glacial lake outburst floods being a key mechanism (13) during glacier retreat. These glacial erosion processes would likely have increased with the intensification of glacial cycles in the last 1 Ma (14), coincident with the increased wood burial inventory provided here. Undersea transport is also likely to be very different in the last 1 Ma as glacial-interglacial sea level rise and fall of up to 120 m would have altered the mobilization of material from shelf to the fan as described for the Indus (15) and Bengal Fans (16). In summary, in the last 1 Ma, we observe abundant and frequent wood

horizons, and diverse chemical composition, suggesting variable environments and erosion processes moving material from varied ecosystems and parts of the catchment, with the episodically exported wood buried with the coarse-grained turbidites of the Bengal Fan.

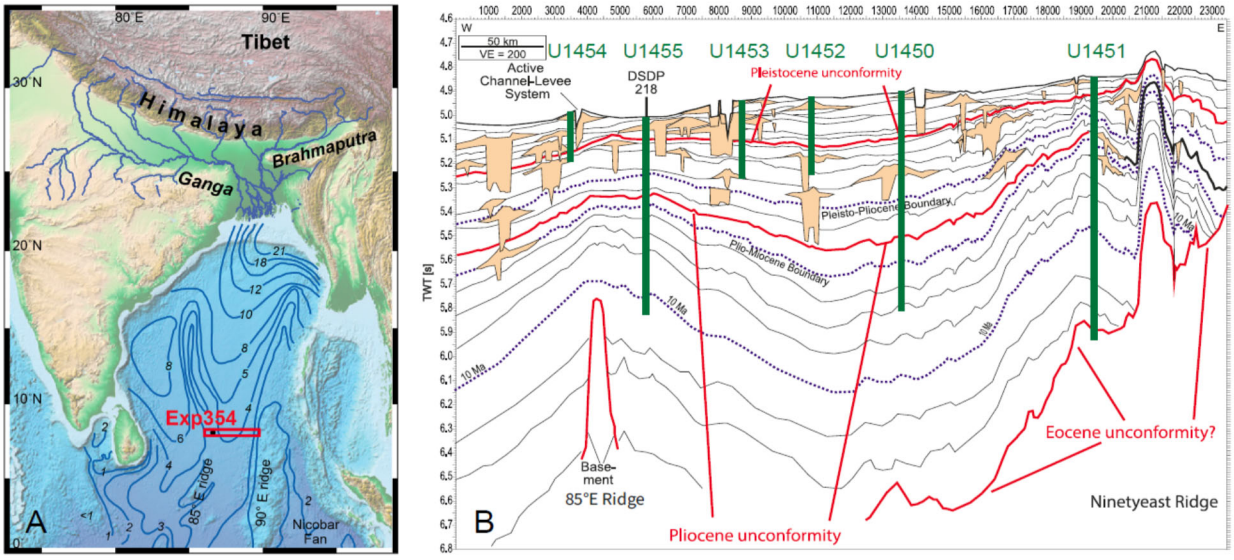

Supplemental Fig. S1. Maps of IODP Exp 354 cores analyzed in this study, modified from (17). *(A)* Map of the Himalayan erosion system showing the G-B Rivers, the location of Expedition 354 transect at 8°N (boxed region). The Bengal Fan sediment isopachs (blue lines; in kilometers) are simplified from (18) and represent the total sedimentary and metasedimentary rocks above the oceanic basalt as interpreted from seismic reflection and refraction data. Colors denote elevation, lowlands (0-200 m) are indicated in shades of green. *(B)* Six cores sampled in this study overlaid on interpreted line drawing of Profile GeoB97-020/027, showing the later stage channel-levee systems, regional unconformities, and faults.VE = vertical exaggeration. TW = two-way travel time. Horizontal scale = CMP, CMP distance = 20 m.

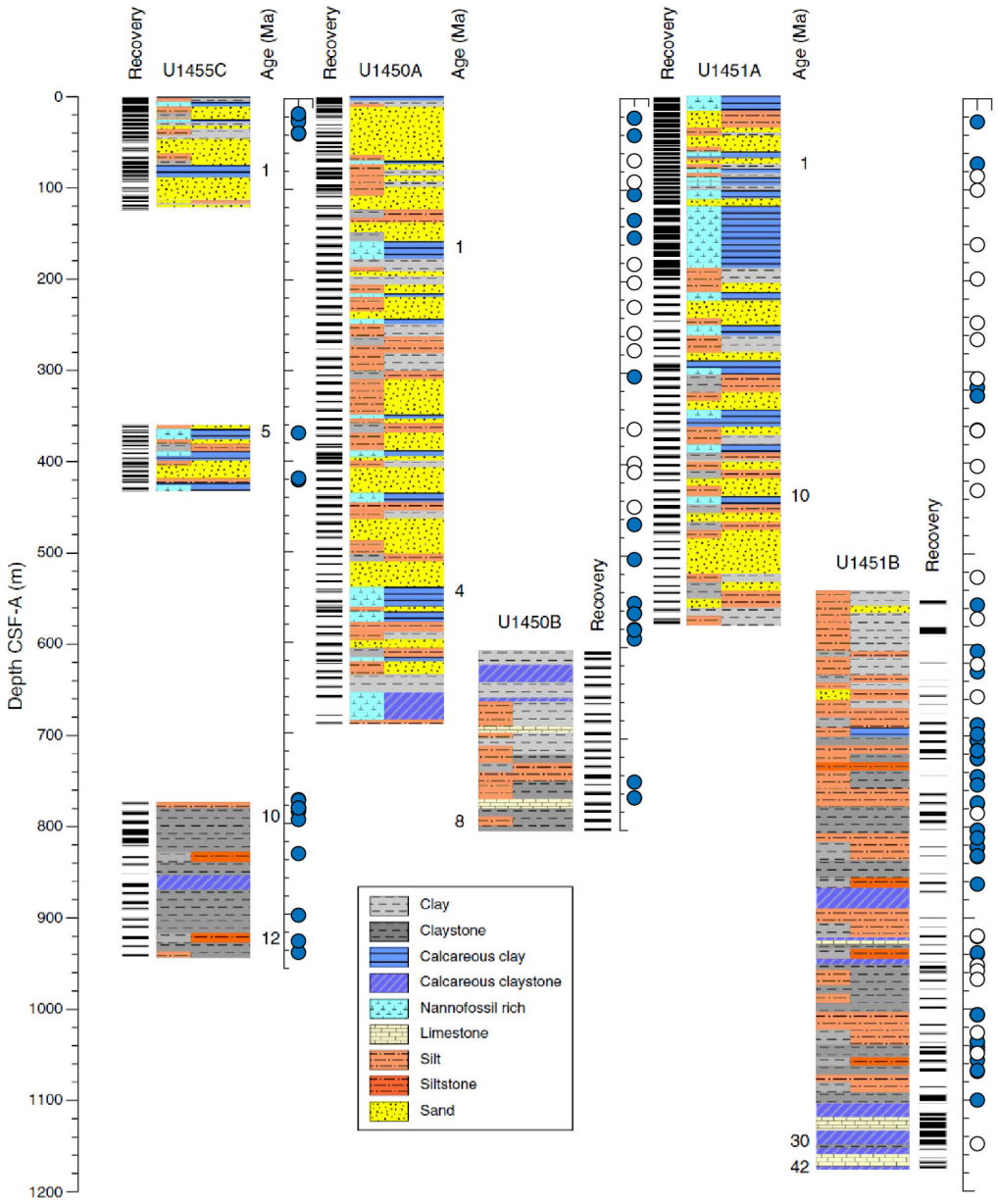

Supplemental Fig. S2. Wood fragments (blue symbols) and barren samples (open symbols), displayed alongside stratigraphic position; Exp 354 stratigraphic columns modified from (17).

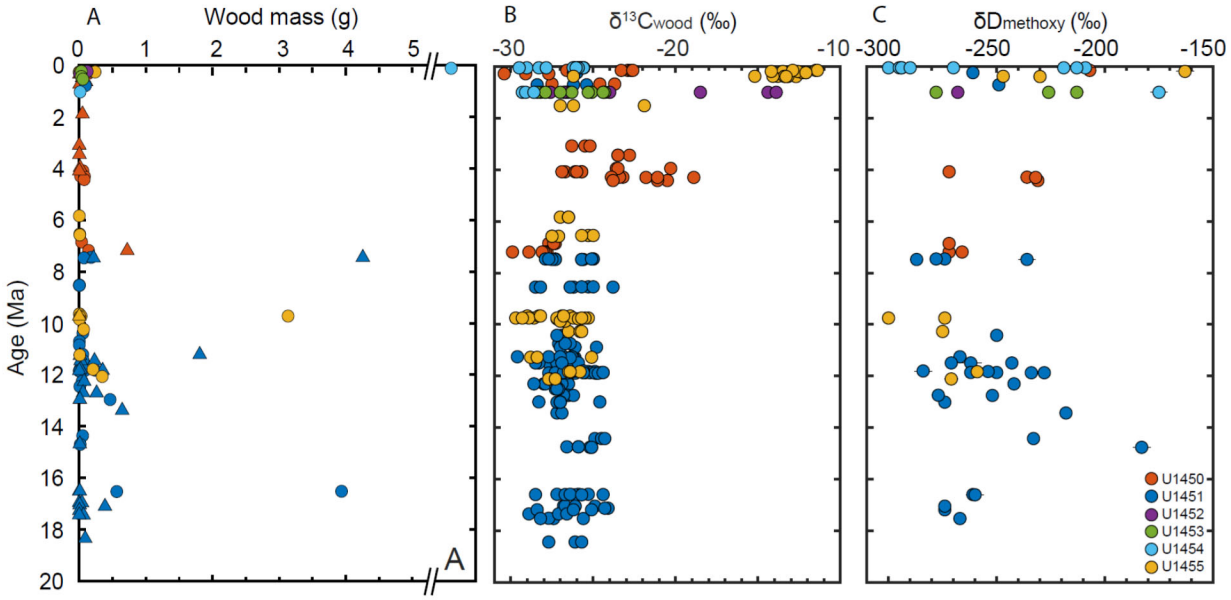

Supplemental Fig. S3. Occurrence and isotopic composition of wood in IODP Expedition 354 Sites U1450, U1451, U1452, U1453, U1454, U1455 in the Bengal Fan (color of symbol denotes Site – see legend on *C*, circle indicates picked sample, triangle indicates sieved sample, showing only those samples that yielded wood). *(A)* Total wood mass per sample in log scale from two datasets: those wood fragments picked from shipboard visual inspection of split cores, and fragments sieved and picked from 10 – 80 g of sediments post-expedition *(B)* Carbon isotopic composition of wood ($\delta^{13}C_{wood}$). *(C)* Hydrogen isotopic composition of lignin methoxy ($\delta D_{methoxy}$).

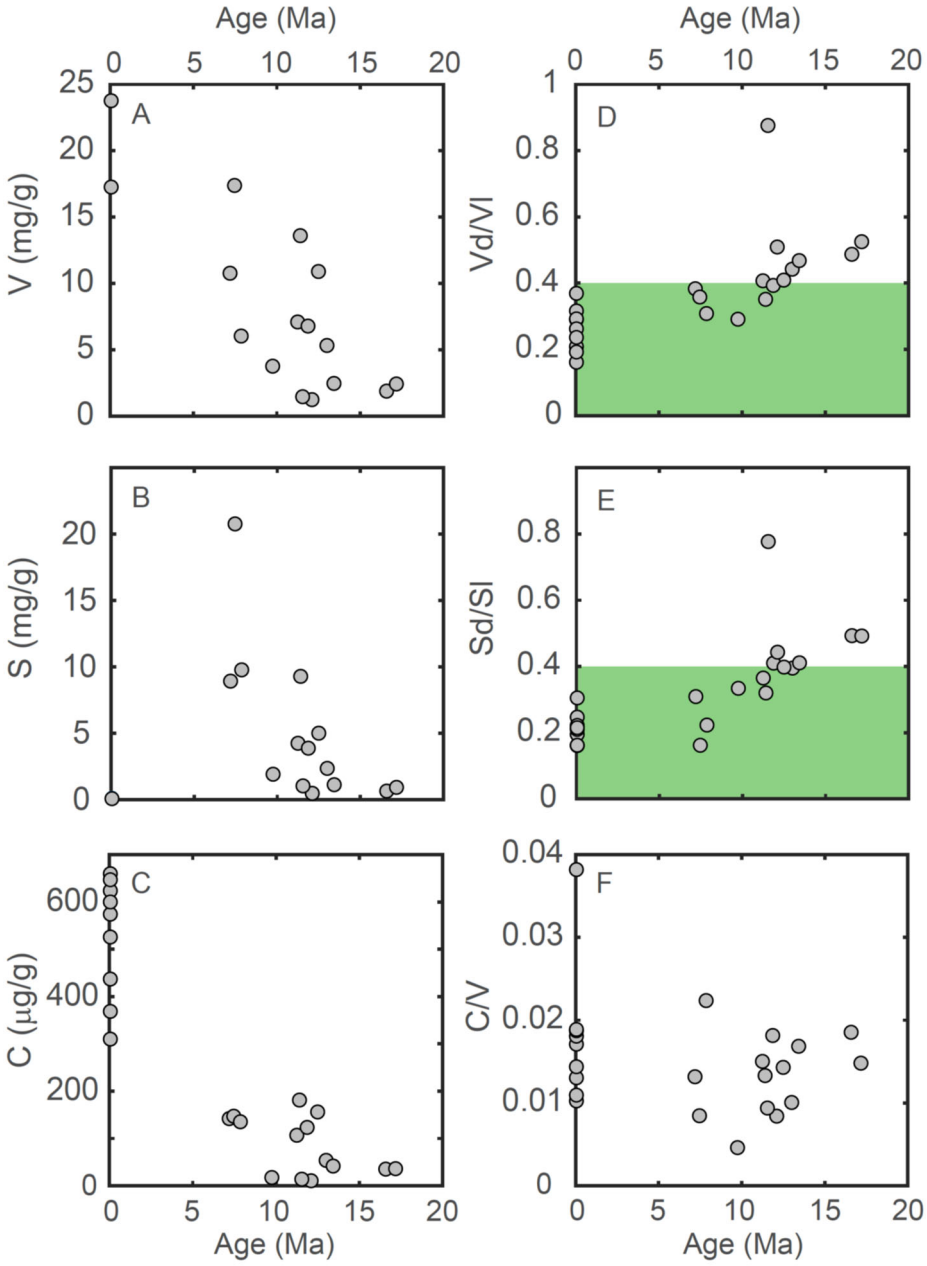

Supplemental Fig. S4. Ratios and concentrations of major lignin phenol groups in Bengal Fan buried wood fragments. Phenol concentrations of *(A)* vanillyl (V) group *(B)* syringyl (S) group and *(C)* cinnamyl (C) group. [V], [S], and [C] concentrations decline with age, yet the larger decrease in S compared to V results in the decline in S/V ratios with age shown in Fig. 3, interpreted in terms of progressive degradation based on the data in panels A-E here. Acid to aldehyde ratios for *(D)* the V (Vd/Vl) and S group phenols (Sd/Sl). Acid/aldehyde ratios increase with age revealing progressive degradation. Overall the samples are remarkably well preserved, with samples within the last 12 Myr, falling within the values <0.4 typical of fresh wood (green shading). *(F)* Ratio of C to V phenols (C/V). Low C/V ratios (<0.05) confirm that the samples are sourced from woody not leafy tissues.

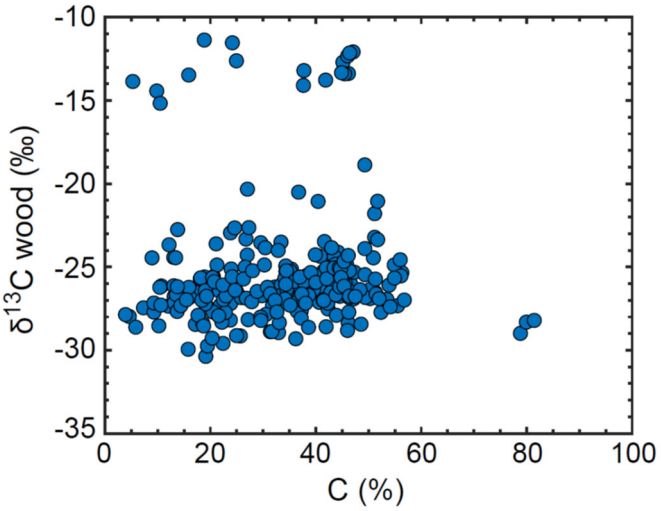

Supplemental Fig. S5. Bulk organic carbon properties of Bengal Fan wood fragments: carbon vs. carbon isotopic composition. Low C implies matrix dilution or water adsorption. Three samples with elevated C (~80%) are inferred to be charcoal.

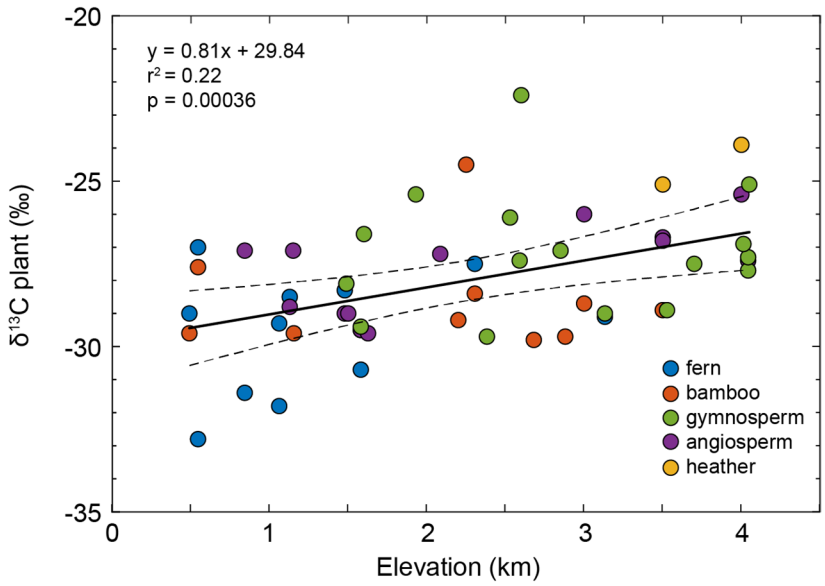

Supplemental Fig. S6. Modern C_3 plant survey of woody branch tissue $\delta^{13}C$ values across an elevation transect in Arunachal Pradesh, India and Central Nepal. We observe an overall tendency to ^{13}C-enrichment with elevation of +0.8‰ km^{-1} ($r^2 = 0.22$, $p = 0.00$). Plant types have distinct elevation ranges, and are shown for illustrative purposes, although we find no systematic difference between plant type (fern, graminoid (bamboo), gymnosperm tree, angiosperm tree/shrub), with the exception of two heather samples that are notably ^{13}C-enriched relative to other angiosperms at that elevation, including other shrubs. One C_4 grass at 1.5 km was excluded from the C_3 elevation trend presented here (*SI Appendix,* Dataset S6).

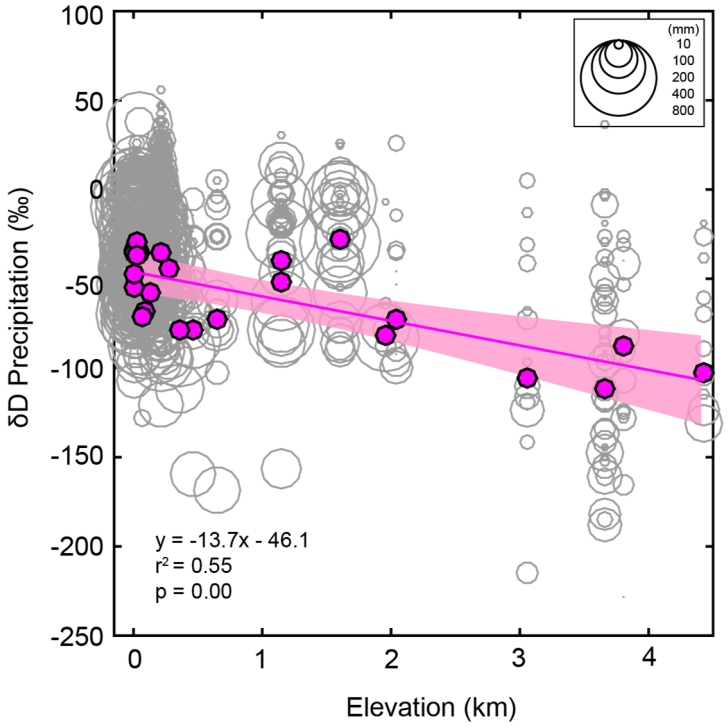

Supplemental Fig. S7. Monthly δD_{precip} plotted against elevation from a selection of Global Network of Isotopes in Precipitation (GNIP) stations in the G – B catchment (Gangotri, Gomukh, Dobrani, Maneri, Uttarkashi, Tehri, Devprayag, Rishikesh, Roorkee, Nainital, New Delhi, Lhajung, Lhasa, Lucknow, Allahabad, Patna, Dinajpur, Guwahati, Dhaka, Sylhet, Shillong, Barisal, Chuadanga, Kolkata, Satkhira – see *SI Appendix, Dataset S5*) (19). Grey circles indicate individual data with sizes scaled to precipitation amount. At every altitude, there is a large isotopic spread (>100 ‰) due to seasonal variability with the Indian Summer Monsoon. Elevation trend in weighted mean annual precipitation δD (magenta circles) is -13.7‰/km (r^2 = 0.55, p <0.0001) based on ordinary least squares linear regression (line), showing 95 % confidence interval (shading).

Dataset S1 (separate file)
Bengal Fan wood mass recovered

Dataset S2 (separate file)
Bengal Fan wood lignin phenol concentrations

Dataset S3 (separate file)
Bengal Fan wood organic carbon concentrations and carbon isotope measurements

Dataset S4 (separate file)
Bengal Fan wood lignin methoxy hydrogen isotope measurements

Dataset S5 (separate file)
Map of locations referenced in this study

Dataset S6 (separate file)
Arunachal Pradesh (India) and Central Nepal elevation transects to survey of woody plant carbon isotopic composition.

Supplemental References

1. H. Lee, X. Feng, M. Mastalerz, S. J. Feakins, Characterizing lignin: Combining lignin phenol, methoxy quantification, and dual stable carbon and hydrogen isotopic techniques. *Org. Geochem.* **136**, 103894 (2019).
2. T. Ma *et al.*, Divergent accumulation of microbial necromass and plant lignin components in grassland soils. *Nat. Comm.* **9**, 3480 (2018).
3. J. I. Hedges, D. C. Mann, The characterization of plant tissues by their lignin oxidation products. *Geochim. Cosmochim. Ac.* **43**, 1803-1807 (1979).
4. S. C. Thomas, A. R. Martin, Carbon content of tree tissues: a synthesis. *Forests* **3**, 332-352 (2012).
5. P. A. Meyers, R. Ishiwatari, Lacustrine organic geochemistry—an overview of indicators of organic matter sources and diagenesis in lake sediments. *Org. Geochem.* **20**, 867-900 (1993).
6. P. D. Clift, Controls on the erosion of Cenozoic Asia and the flux of clastic sediment to the ocean. *Earth Planet. Sci. Lett.* **241**, 571-580 (2006).
7. J. Nie *et al.*, Rapid incision of the Mekong River in the middle Miocene linked to monsoonal precipitation. *Nat. Geosci.* **11**, 944-948 (2018).
8. L. Diester-Haass *et al.*, Mid-Miocene paleoproductivity in the Atlantic Ocean and implications for the global carbon cycle. *Paleoceanography* **24**, PA1209 (2009).
9. U. Siegenthaler *et al.*, Stable carbon cycle-climate relationship during the late Pleistocene. *Science* **310**, 1313-1317 (2005).
10. S. Eggleston, J. Schmitt, B. Bereiter, R. Schneider, H. Fischer, Evolution of the stable carbon isotope composition of atmospheric CO_2 over the last glacial cycle. *Paleoceanography* **31**, 434-452 (2016).
11. C. J. Hein *et al.*, Post-glacial climate forcing of surface processes in the Ganges–Brahmaputra river basin and implications for carbon sequestration. *Earth Planet. Sci. Lett.* **478**, 89-101 (2017).
12. S. Weldeab, C. Rühlemann, B. Bookhagen, F. S. R. Pausata, F. M. Perez-Lua, Enhanced Himalayan Glacial Melting During YD and H1 Recorded in the Northern Bay of Bengal. *Geochem. Geophys. Geosyst.* **20**, 2449-2461 (2019).
13. K. L. Cook, C. Andermann, F. Gimbert, B. R. Adhikari, N. Hovius, Glacial lake outburst floods as drivers of fluvial erosion in the Himalaya. *Science* **362**, 53-57 (2018).
14. L. Lisiecki, M. Raymo, A Pliocene-Pleistocene stack of 57 globally distributed benthic $\delta^{18}O$ records *Paleoceanography* **20**, 1-17 (2005).
15. J. Bourget *et al.*, Late Quaternary megaturbidites of the Indus Fan: Origin and stratigraphic significance. *Mar. Geol.* **336**, 10-23 (2013).
16. M. E. Weber, M. H. Wiedicke, H. R. Kudrass, C. Hübscher, H. Erlenkeuser, Active growth of the Bengal Fan during sea-level rise and highstand. *Geology* **25**, 315-318 (1997).
17. C. France-Lanord *et al.*, Expedition 354 Summary, *Proceedings of the Ocean Drilling Program* **354**, 1-35 (2016).
18. J. R. Curray, F. J. Emmel, D. G. Moore, The Bengal Fan: morphology, geometry, stratigraphy, history and processes. *Mar. Pet. Geol.* **19**, 1191-1223 (2003).
19. IAEA/WMO (2019) Global Network of Isotopes in Precipitation. The GNIP Database. Accessible at: http://www.iaea.org/water. (Date of access: 7/12/2018)